JTTEE5 10:326-336

Spectroscopic Temperature Measurements in Direct Current Arc Plasma Jets Used in Thermal Spray Processing of Materials

S. Semenov and B. Cetegen

(Submitted 29 June 2000; in revised form 19 September 2000)

An experimental study was conducted to determine the plasma temperature field and its parametric variation with respect to plasma operating conditions using emission spectroscopy. The focus of our study was the direct current (DC) arc plasma systems used in thermal spray processing of ceramic materials. A commercial plasma system (Metco 9M series) was operated with mixtures of argon and hydrogen in the power input range from 12 to 36 kW. Temperature measurements were based on the detection of emission line intensities from Ar-I neutral species. Spatially resolved measurements were obtained of the plasma temperatures in axisymmetric plasma jets using Abel deconvolution. The variation of plasma axial and radial temperature distributions was measured as a function of the plasma input power, the total gas flow rate, and the binary gas composition of argon and hydrogen. Time-averaged plasma gas temperatures were found to increase with increasing plasma input power, increasing hydrogen content of the plasma gas, and decreasing total gas flow rate. Plasma temperatures decrease progressively with increasing distance from the nozzle exit. The peak temperatures near the nozzle exit are in the range of 12,500 to 14,000 K. The radial temperature profiles show an approximately self-similar decay in the near field of these plasma jets. It was also determined from time resolved intensity measurements that there are significant fluctuations in the argon emission intensity with increasing hydrogen fraction in the mixture. These fluctuations with a typical frequency of 5.2 kHz are attributed to the arc root instabilities observed before. Finally, the measured plasma temperature field is empirically correlated in terms of radial and axial coordinates, plasma electrical input power, plasma efficiency, and gas composition. These temperature data can be used to validate numerical simulations as well as in choosing locations where different materials can be introduced into the plasma jets. This is particularly important for "nanostructured" materials, which loose their structure upon melting as a result of being exposed to high plasma temperatures.

Keywords diagnostics, imaging, plasma spectroscopy, temperature field

1. Introduction

One of the well-known applications of plasma processing is the application of high-temperature materials onto substrate surfaces to form high-temperature resistant coatings.[1] This process commonly referred to as "plasma thermal spray" has been in existence for many years. The process involves introduction of the coating material into a plasma jet in the form of a powder stream or wire feed and subsequent heatup and melting of this material before impacting onto a substrate to be coated. Typically, the materials suitable for plasma thermal spray process are those with high melting temperatures that require heating sources with temperatures significantly higher than those obtained in combustion of hydrocarbon fuels in oxygen, limited to adiabatic flame temperatures of about 2500 K. In plasmas, gas temperatures up to 15,000 K can be attained, thereby enabling melting of ceramic materials. In the direct current (DC) arc plasma systems commonly used in this field, an electrical arc is formed between the anode and cathode of a plasma nozzle assembly through which an inert gas flows, as shown schematically in Fig. 1. In order to control the plasma properties, small amounts of hydrogen or helium gas are used as well. Materials are typically injected external to the plasma nozzle, as shown in Fig. 1. So far, axial injection of materials inside the plasma nozzle has been difficult and problematic at best, although there are some new DC arc plasma systems which are capable of axial injection of powders. In material processing by plasma jets, one of the key process parameters is the plasma temperature field to which the material is exposed as it is injected into the plasma stream, necessitating a knowledge of the plasma thermal environment. An accurate knowledge of the plasma thermal environment is even more important when high value nanostructured coating materials are used in plasma thermal spraying due to the temperature sensitivity of these materials to phase transformation and loss of nanostructure upon melting.

A detailed and complete knowledge of plasma temperature field and its dependence on the plasma operating parameters such as nozzle configuration and design, electric power input, and plasma gas flow rates therefore are needed. This knowledge is a prerequisite for accurately determining particle heatup in plasma thermal spray processes. Due to the very high temperatures attained in DC arc plasma jets, a spectroscopic technique is most suitable for measurement of plasma temperatures. Al-

S. Semenov and **B. Cetegen,** Mechanical Engineering Department, University of Connecticut, Storrs, CT 06269-3139. Contact e-mail: cetegen@engr.uconn.edu.

Nomenclature

A_{ij}	transition probability of *i* to *j* transition, sə[1]
C_w	water specific heat, J/(kg·K)
d	nozzle diameter, m
g_i	statistical weight of an atom in the i[th] excited state
h	Plank constant, J·s
I_{ij}	absolute intensity of the emission line, W/(m²·s)
k	Boltzmann constant, J/K
L	emission source depth, m
m_w	water mass flow rate, kg/s
n_i	electron population of the *i*[th] atom excited state
P_{el}	electrical input power, W
R	intensity ratio
T	absolute temperature, K
T_{cl}	centerline plasma temperature, K
T_∞	ambient temperature taken as 300 K
V_{Ar}	argon volumetric flow rate, m³/s
Y	mole fraction
z	axial distance, m
Z	partition function

Greek symbols

ε_i	excitation energy, J
η_{pl}	plasma torch efficiency
λ	wavelength, nm
γ_{ij}	photon frequency for electron transition from *i* to *j* level, Hz

Subscripts

i, j	different energy levels

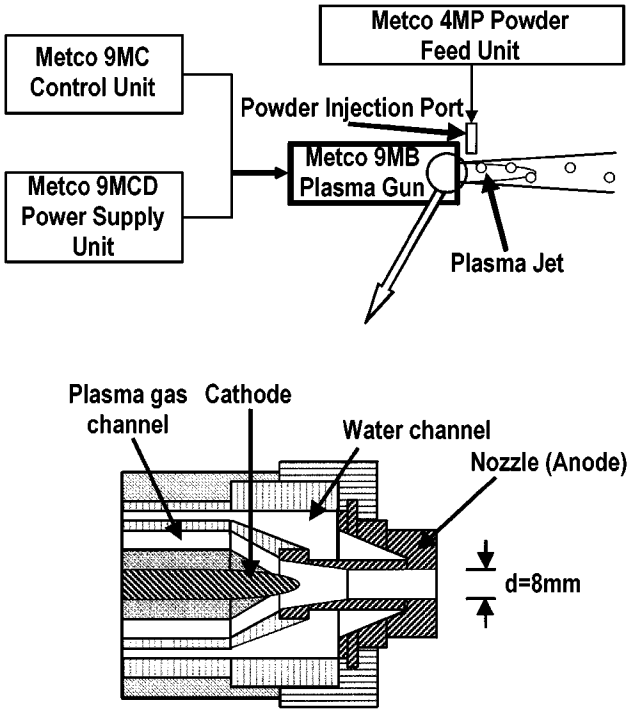

Fig. 1 Experimental setup showing the Metco DC arc plasma system components and the nozzle detail

though probing techniques have been applied to measure plasma temperature and species such as enthalpy probes,[2] their use is cumbersome at best and such techniques are not conducive to *in-situ* monitoring and control of plasma state, particularly when one considers the feedback control of plasma thermal environment. For example, the nonintrusive optical techniques such as emission spectroscopy can be employed to monitor the plasma gas temperatures upstream of the powder injection point.

In general, different types of plasma temperature have been identified. These include (1) electron temperature determined from the kinetic energy of the electrons, (2) gas temperature reflecting the kinetic energy of the neutral atoms or molecules, (3) excitation temperature related to the population of the various electronic energy levels, and (4) ionization temperature governing the ionization equilibrium. These different measurements in a plasma environment can have different values unless the plasma is in local thermodynamic equilibrium. All temperatures approach a common value when the condition of local thermodynamic equilibrium (LTE) is reached. In the atmospheric pressure plasmas studied here, the LTE exists because of (1) the small values of the parameter E/P, where E is the electric field strength and P is the pressure,[3] and (2) existence of excitation equilibrium among different energy levels, as shown later from our measurements. Since LTE exists in the studied plasmas, the measured excitation temperatures also correspond to the gas temperature defined by the kinetic energy of the bulk neutral species.

In the plasma literature, temperature measurements have been made using emission spectroscopy of excited plasma gas species. The employed techniques include the Boltzmann method,[4,13] the modified Boltzmann method,[5] the absolute intensity method,[6] the method based on measurement of the intensity ratio of two lines,[4,12] and Thomson laser-light scattering.[7,8] In this study, the Boltzmann method was adopted to measure plasma temperature field based on the population of Ar-I species distributed in different electronic states. While these techniques had been used in the past[4,5,9] for plasma characterization, we have extended this measurement technique in this study to the determination of plasma temperatures along thin slices across the plasma width (or diameter), thus allowing capture of the temperature profiles along the full radial extent of the plasma jet. The radial distributions of plasma temperatures are particularly useful for external transverse injection of powder into DC arc plasmas in determining particle heatup. Our effort in this study focused on the effects of plasma electrical power input, plasma gas composition, and total plasma gas flow rate on the temperature field of the Ar-H_2 plasmas. The experimental results are presented in empirical correlations that can be useful for comparisons with calculations as well as using the experimental temperature data for thermal spray process optimization. In the following, we first describe the commercial plasma system that was used for the described measurements. This is followed by a description of the optical setup for the temperature measurements. The experimental results are presented and discussed subsequently.

Table 1 Ar-I neutral species electronic transition parameters

λ, nm	A_{ij}10,^{6},s^{-1}(a)	g_i(b)	E_{ij}, cm^{-1}(c)
418.188	0.56	3	118,459.662
419.103	0.54	3	118,407.494
419.832	2.57	1	117,563.020
420.067	0.97	7	116,942.815
425.118	0.11	3	116,660.054
425.936	3.98	1	118,870.981
426.629	0.31	5	117,183.654
427.217	0.80	3	117,151.387

(a) Transition probability of the *i* to *j* transition from Ref 10
(b) Statistical weight from Ref 14
(c) Excitation energy in wavenumbers from Ref 14

2. Experimental

2.1 DC Arc Plasma System

A stationary plasma jet was produced by a commercial DC arc plasma system (Metco, model 9M, Westbury, NY) consisting of the plasma torch (Metco, model MB) equipped with a GH water-cooled copper anode nozzle, the plasma control unit (Metco, model 9MC), and the plasma power supply (Metco model 9MCD), as shown schematically in Fig. 1. In this configuration, a gas mixture of argon and hydrogen passes through the arc gap, where a continuous DC arc heats the gas stream before it exits through an 8.0 mm diameter nozzle. The argon-hydrogen gas mixtures had a volumetric fraction of argon ranging between 80 and 100%. The remaining portion was hydrogen used to change the arc breakdown characteristics as well as thermal properties of the plasma. The plasma input power, P_{el}, can be determined based on the measured potential difference across anode and cathode, ΔV, and the controlled and measured current, I, as $P_{el} = I(\Delta V)$. The plasma gun was operated at three nominal input power levels of 12, 24, and 36 kW with total gas flow rates between 2.83 and 4.25 m^3/h. In all experiments, plasmas discharged into atmospheric air.

2.2 Spectroscopic Technique for Plasma Temperature Measurements

Among the different techniques for temperature measurement, the spectral emission from the excited Ar-I neutral species was selected due to the strong emission of Ar-I species in the visible region ranging from 418 to 427 nm, as listed in Table 1, obtained from Wiese *et al.*[10] Up to eight Ar-I emission lines can be detected with the optical setup described below. Properly corrected emission intensities can be used to determine the temperatures based on the Boltzmann distribution given by

$$n_{oi} = n_o \frac{g_i}{Z} \exp(-\varepsilon_i / kT) \quad \text{(Eq 1)}$$

where n_{oi} is the population of the ith excited state, g_i is the known statistical weight or degeneracy of the excited state, Z is the partition function, ε_i is the excitation energy, k is the Boltzmann constant, and T is the absolute temperature The absolute intensity of the emission line can be written as

$$I_{ij} = \frac{l}{4\pi} A_{ij} n_{oi} h\nu_{ij} \quad \text{(Eq 2)}$$

where l is the emission source depth, A_{ij} is the transition probability of i to j transition, and $h\nu_{ij}$ is the energy of transition from i to j. Combining Eq 1 and 2 and taking the natural logarithm yields

$$\ln\left(\frac{I_{ij}}{g_i A_{ij} \nu_{ij}}\right) = \ln\left(\frac{l h n_o}{4\pi Z}\right) - \frac{\varepsilon_i}{kT} \quad \text{(Eq 3)}$$

Based on this relation, a plot of the left-hand side versus the excitation energy, ε_i, would yield a linear relationship with a slope of $(-1/kT)$ since all other terms in Eq 3 are constants. This plot is often referred to as the Boltzmann plot. Another variation of this technique is to use two line intensities with sufficiently different excitation energies to determine the temperature directly from

$$T = \frac{\varepsilon_2 - \varepsilon_1}{k \ln\left(\frac{A_2 g_2 \nu_2 I_1}{A_1 g_1 \nu_1 I_2}\right)} \quad \text{(Eq 4)}$$

as was subsequently employed in our study.

2.3 Optical Setup for Emission Spectroscopy

The experimental setup for spectroscopic measurements of plasma temperature is schematically shown in Fig. 2. A multiple lens assembly (Tamron 70-210 SP) with a variable focal length was used to image the plasma radiation onto the entrance slit of a 0.5 m path length spectrometer (McPherson model 216.5, Acton, MA). The typical focal depth of the imaging optics was 30 mm. The vertically oriented spectrometer slit had a nominal width of 50 μm. Inside the spectrometer, the collimating mirror reflects plasma light on a dispersion grating with 2400 lines/mm. Spectrally dispersed in the horizontal image plane, the plasma radiation is focused by a cylindrical mirror onto a 1035 $\times$ 1317 pixel CCD camera (Photometrics model CE200, Tucson, AZ) at the output port of the spectrometer. The thermoelectrically cooled, 12-bit readout CCD camera was used to capture the spectrally dispersed plasma emission. Analysis of the acquired spectral images was performed using optical multichannel analysis software on a Macintosh computer. Before performing the experiments, the spectral calibration of the spectrometer system including the CCD chip spectral sensitivity was checked using the scattered light at different emission wavelengths of an Argon ion laser. The throughput rate of the optical system was also checked by traversing the light source along the slit length and recording the spectrometer output. It was found that the throughput of the optical system had a maximum variation of 1.4%.

In the experiments, the CCD camera exposure time typically ranged between 70 ms and 5 s. Thus, the determined temperatures represent time-averaged values over these time periods. A sensitivity study was performed to determine the influence of time averaging in temperature measurements at several locations. It was found that the plasma temperature field was reasonably repeatable within 4% for averaging times between 70

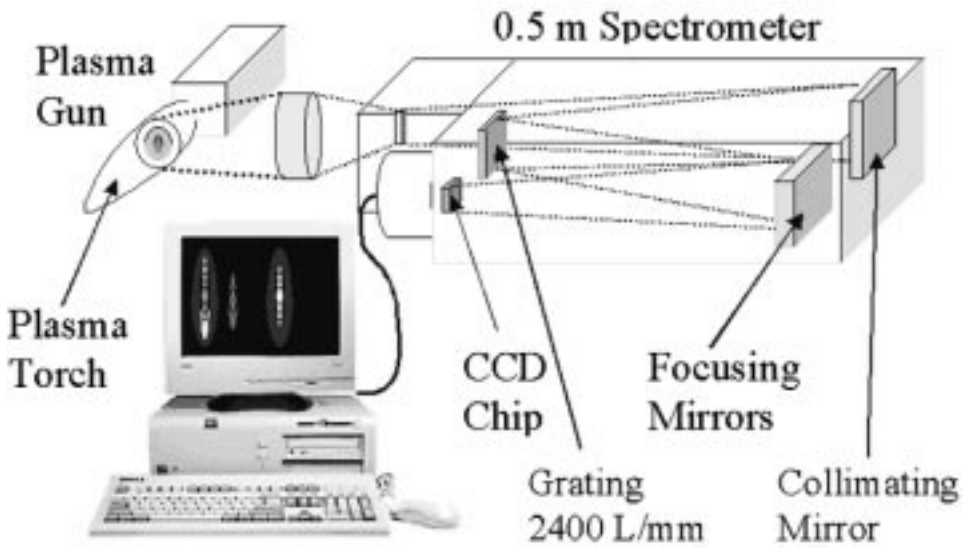

Fig. 2 Schematics of the diagnostics setup used in the emission spectroscopy

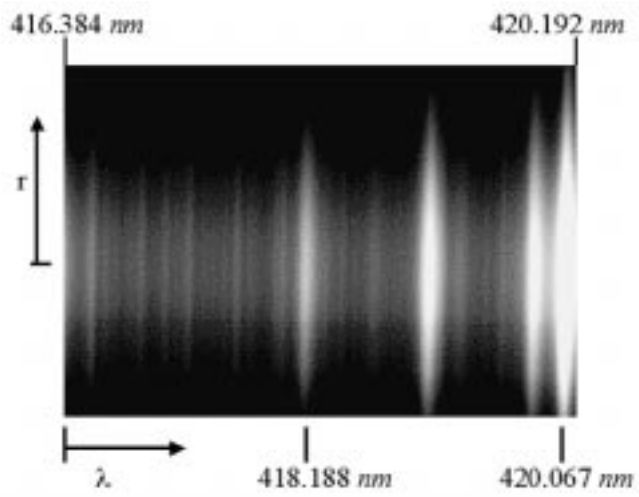

Fig. 3 An example of the Ar-I emission spectrum imaged at the exit plane of the spectrometer

ms and 1.0 s. Up to 20 spectra were taken at some locations to determine the repeatability of the measured line intensities.

Due to the line-of-sight nature of the emission measurements, the measured emission intensities need to be deconvoluted in order to determine local intensities. In the time-averaged measurements along a radial chord of the plasma, this deconvolution takes the form of Abel's inversion using the assumption of axisymmetry.[4] For the plasma jets studied without the transverse particle injection jet, the assumption of axisymmetry is a good one. Hence, the measured emission intensities and the background intensities were first deconvoluted using an "onion-peeling" Abel's inversion scheme[4] after which the temperature calculations were carried out using Boltzmann distribution. In the emission intensity measurements, there appears a broadband background emission due to high-temperature plasma. This background emission is superimposed on the spectral emission intensities of Ar-I lines in the measurements. A proper data analysis procedure involves subtraction of this background intensity from the spectral line intensities, as described in the next section.

Uncertainty in the temperature measurements was assessed based on the uncertainties in the spectral constants for Ar-I transitions as well as in the measurements. It was found that temperature uncertainties can approach 30% based on the time-averaged intensity data when uncertainties in the transition probabilities reported in the literature and used in this work are combined with the measurement uncertainty of the line emissions. The uncertainties at high-intensity and high-temperature regions are dominated by the uncertainties in transition probability, whereas the uncertainty in the lower temperature regions is controlled by the uncertainty in the measured intensities. Based on the uncertainty of the measured spectral intensities alone, the uncertainty in the determined temperature is around 10%.

Finally, argon emission intensity at $\lambda = 420.07$ nm was recorded by a fast photomultiplier detector to characterize plasma fluctuations. These fluctuations were recorded as a function of plasma power and gas composition to reveal the time dependence of the spectral emission from the plasma, which was not possible in the experimental setup described earlier.

3. Results and Discussion

Experimental results on the plasma temperature field by emission spectroscopy are described and discussed in this section. First, the results obtained based on the full Boltzmann spectral analysis are presented. The procedure of experimental data reduction involved Abel's inversion of the measured Ar-I emission lines and background intensities. Figure 3 shows an image of the spectrometer output where up to 10 Ar-I emission lines covering 404 nm $< \lambda <$ 435 nm can be identified. After the

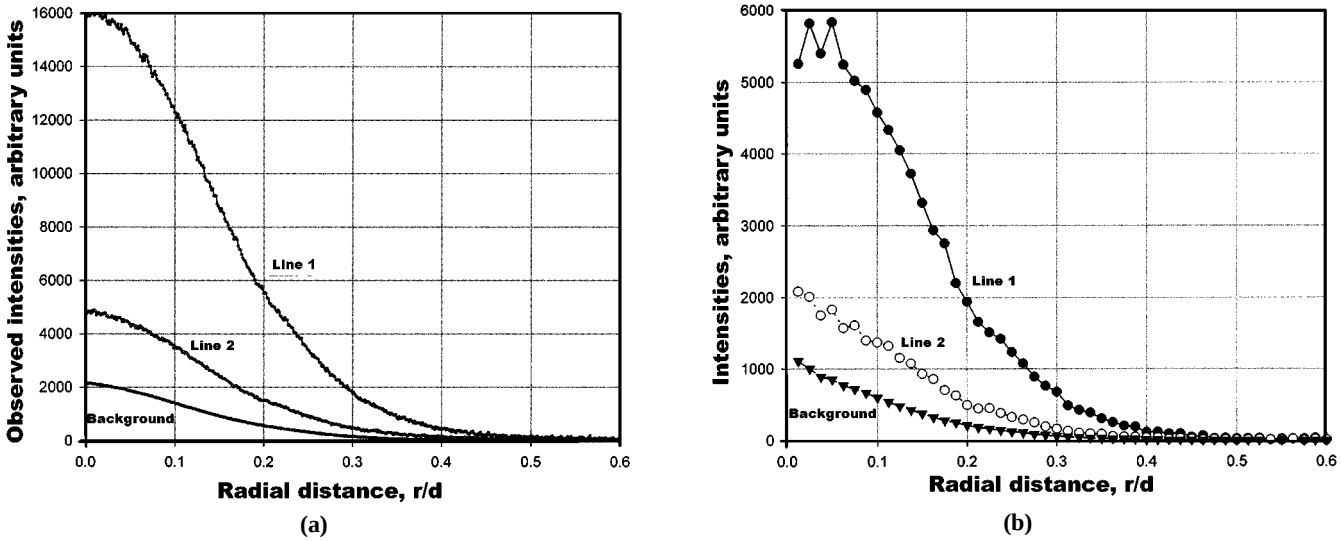

Fig. 4 Radial profiles of Ar-I emission intensities at $\lambda = 418.188$ and 420.067 nm and background: (**a**) line of sight as measured and (**b**) deconvoluted using Abel's inversion

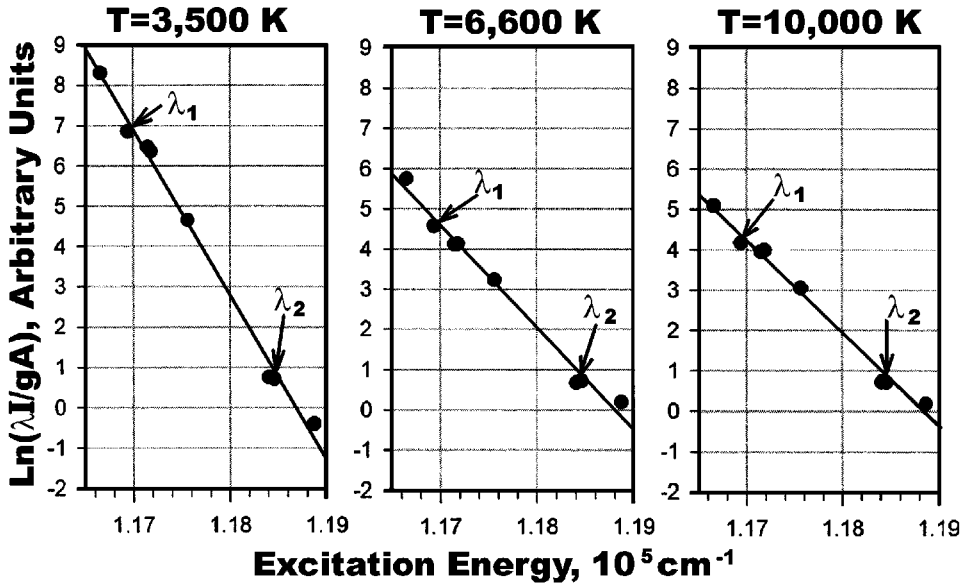

Fig. 5 Three examples of Boltzmann plots at three different locations in a 12 kW Ar/H_2 plasma jet

Abel's inversion of these line intensities and the associated background intensities, the absolute intensities, $I = I_{measured} - I_{background}$, were used to construct the Boltzmann plots. Examples of the distributions of the measured line-of-sight emission intensities and the background intensity are shown in Fig. 4(a). These data were first smoothed out by a ten-point moving average scheme and then deconvoluted using an onion-peeling Abel's inversion scheme.[4] The inverted intensities are shown in Fig. 4(b) corresponding to those shown in Fig. 4(a). In all the deconvolution schemes, the inverted data suffer from some degree of scatter near the centerline. This required additional smoothing of the data in these regions. The particular onion-peeling approach produced similar results to the two-point numerical differentiation approach of Dash.[11] Boltzmann plots at several different locations in the plasma are shown in Fig. 5. As seen in this figure, the resulting Boltzmann plots are of very high quality with the slope of the linear relationship through the data producing an unambiguous plasma temperature. The three examples of Boltzmann plots were obtained from different regions of the plasma, demonstrating the good capability to measuring temperatures over a wide range.

For rapid diagnostic use of this technique for temperature measurements in practical plasma systems, two Ar-I emission lines with sufficiently different excitation energies were chosen in the subsequent measurements. This two-color version of the technique can be used to obtain temperatures explicitly, as given

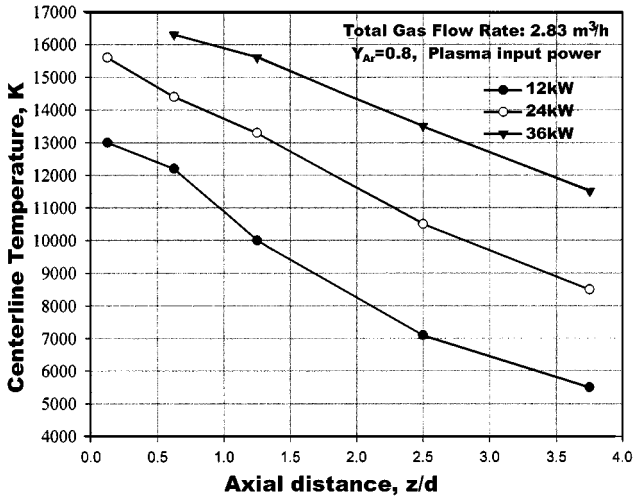

(a)

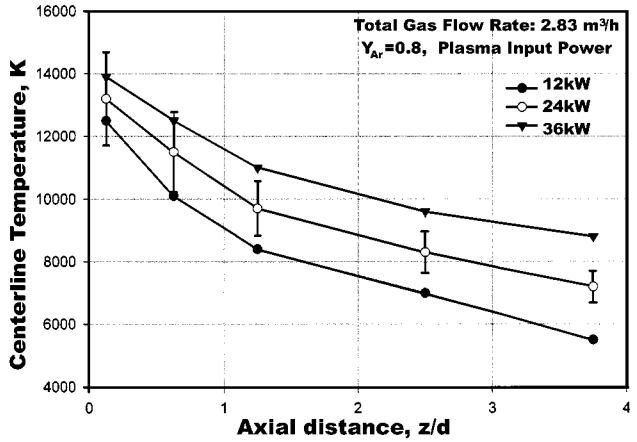

(b)

Fig. 6 Axial distribution of plasma temperatures at three different plasma input power levels. Total plasma gas flow rate = 2.83 m³/h and argon mole fraction = 0.8: (**a**) based on the line-of-sight intensities and (**b**) based on the Abel deconvoluted local intensities. The representative error bars shown are based on the uncertainty in the measured line intensities only

by Eq 4. The line pair chosen for these measurements is at wavelengths of $\lambda = 420.067$ nm and $\lambda_2 = 418.188$ nm. This selection was based on the stronger intensities of these lines compared to others as well as the significantly different excitation energy levels of these transitions, as indicated in Fig. 5. The additional advantages include the small wavelength separation enabling the observation of these lines simultaneously by the spectrometer, negligible variation on the CCD detector quantum efficiency due to small wavelength separation, and the absence of line overlap with adjacent lines.

The data reduction procedure for the measurements to be discussed was as follows. The radial line intensities were first deconvoluted using an onion-peeling Abel's inversion procedure.[4] The deconvoluted intensity profiles for the two emission lines as well as their respective backgrounds were used to calculate the intensity ratios $R = (I_1 - I_{1,\text{back}})/(I_2 - I_{2,\text{back}})$ at each radial location. It was found that Boltzmann plots based on the line-of-sight intensity data resulted in significantly more scatter compared to the examples shown in Fig. 5.

Figure 6 shows the axial variation of plasma temperatures at three plasma power input levels of 12, 24, and 36 kW with an argon volume fraction of 0.8 and an argon flow rate of 2.83 m³/h. Without the Abel's inversion of the line intensities, the determined plasma temperatures are not localized, but they are influenced by differing temperature regions across the plasma cross section. These results in Fig. 6(a) show a rapid decay of temperature with increasing downstream distance due to entrainment of cool ambient air into the plasma jet. In this case, the temperatures closest to the nozzle exit situated near $z/d = 0.0$ range between 13,000 and 17,000 K, which are too high compared to other measurements of temperature in similar plasma systems operating under comparable conditions.[9] This is believed to be due to the errors introduced as a result of using the line-of-sight integrated plasma intensities in the temperature calculation. The centerline plasma temperature distributions obtained after the intensities are first deconvoluted using Abel's inversion are shown in Fig. 6(b). It is found that the initial plasma temperatures are now in the more reasonable range of 12,500 to 14,000 K as a function of the plasma power input. These values are consistent with the other reported plasma exit temperatures under comparable conditions using similar plasma systems.[6,7,9] It is also noted that the axial temperature decay rates are different, with the highest power plasma showing a more gradual decay of plasma temperature as compared to the lowest plasma power. This may be due to the changes in plasma properties (density and viscosity) and their influence on the entrainment characteristics of the plasma. The axial temperature decay in the plasma jet becomes an important factor in determining the axial location at which the powders are injected into the plasma for material processing and thermal spraying of coatings. For example, injection of a ceramic powder transversely into the plasma at $z/d = 1.0$ versus $z/d = 2.0$ could have up to 2000 K temperature differences. This may translate into significant differences in particle heatup as well as different particle material thermodynamic states resulting in melting and vaporization.

The measured plasma temperatures also depend on the plasma gas mixture and the total volumetric gas flow rate through the plasma nozzle. Figure 7 shows the axial variation of the plasma centerline temperature for three values of argon mole fraction (0.8, 0.9, and 1.0) and three different total gas flow rates for a 36 kW plasma power input. It is seen that the measured temperatures increase with increasing hydrogen content of the gas mixture. The temperatures also decrease with increasing total gas flow rate. These variations are related to the change in the enthalpy of the plasma stream, as affected by the plasma heat input, gas flow rates, and composition, as well as the fluctuations discussed later.

In this work, plasma efficiency was determined from the measured heat loss to the cooling water in the plasma torch as

$$\eta_{pl} = 1 - \frac{\dot{m}_w C_w \Delta T_w}{P_{el}} \qquad \text{(Eq 5)}$$

where η_{pl} is the plasma efficiency, m_w and ΔT_w are the measured water mass flow rate and temperature rise across the cooling channel, C_w is the specific heat of the cooling water, and P_{el} is the measured electrical input power. Measured plasma efficiencies are shown in Fig. 8(a) as a function of input power. The re-

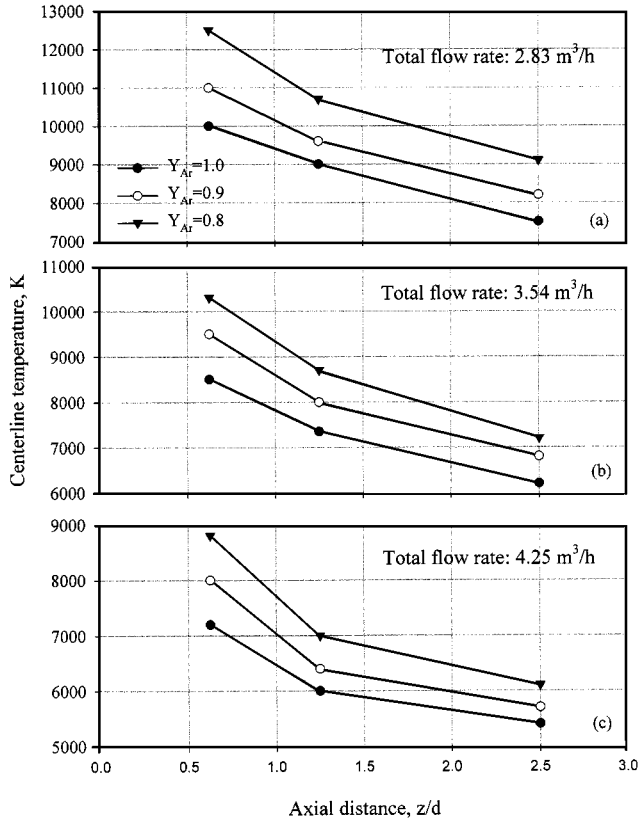

Fig. 7 Effect of plasma gas mixture and total flow rate on the axial distribution of plasma centerline temperatures for 36 kW power input

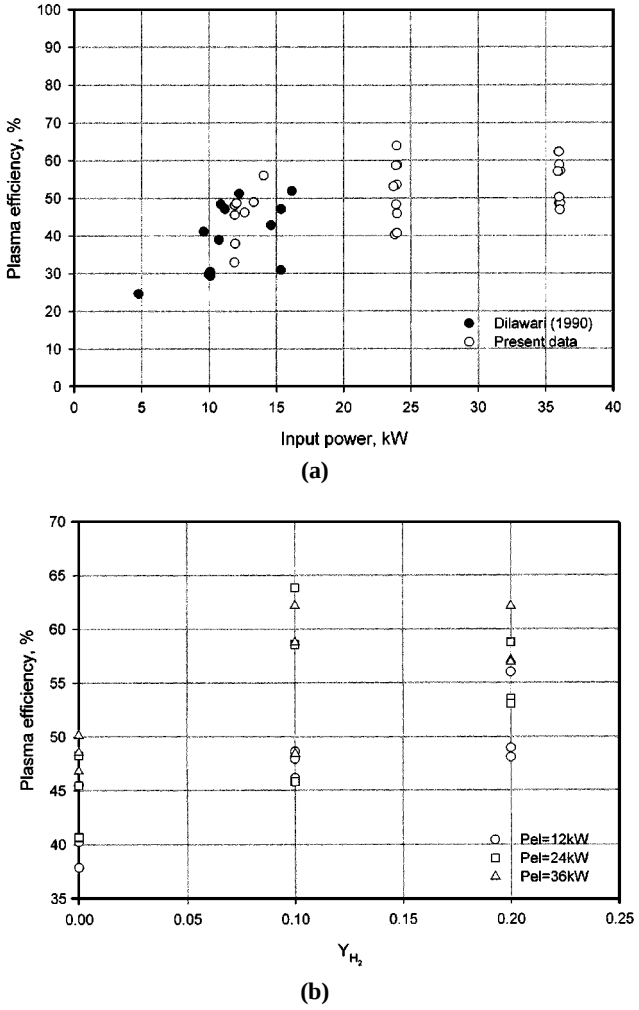

Fig. 8 Plasma thermal efficiency as a function of (**a**) plasma input power and (**b**) plasma gas composition

sults are also compared with the measurements of Dilawari[2,6] at the low power range. It is found that efficiency increases slightly with increasing power, and the agreement with Dilawari data is reasonable given the degree of data scatter. In Fig. 8(b), efficiency is shown as a function of plasma gas composition at three input power levels. It is observed that the efficiency increases somewhat with increasing hydrogen content, although the data scatter is significant.

One of the main objectives of our plasma thermal characterization was to provide a useful correlation for the plasma temperature field for the practitioner. To this end, correlation of plasma temperatures was sought in terms of plasma power, efficiency, gas flow rates, and composition. Figure 9 shows four different empirical correlation parameters in the form of $(P_{th})^n/V_{Ar}$, where $P_{th} = P_{el}\eta_{pl}$ for the following values of the exponent *n:* 1, 1/2, 1/3, and 1/4. The basic form of this parameter relates to the energy density of the plasma. As shown in Fig. 9, it was found that the parameter $(P_{el}\eta_{pl})^{1/4}/V_{Ar}$ provided the best overall correlation at all three axial locations ($Z = 5$, 10, and 20 mm) for the plasma centerline temperature data. The correlation coefficient, r^2, was highest for all measurement locations for this particular parameter. Currently, we do not have a plausible physical explanation as to why this particular combination gives the best correlation of the experimental data.

Radial distributions of plasma temperature are shown in Fig. 10 for 12, 24, and 36 kW Ar/H_2 plasmas. In all cases, the peak temperatures at the centerline decay with radial distance outwards as expected. The rate of radial decay decreases with increasing downstream distance. Because of the high degree of uncertainty in the radiant temperature measurement at the tail ends, the full radial temperature profiles were not possible to obtain. If the similarity of the radial profiles is explored, it is found that the collapse of the data is achieved when $(T - T_\infty)/(T_{cl} - T_\infty)$ is plotted versus z/d, where d is the nozzle diameter and $T_\infty = 300$ K, as shown in Fig. 11. While the degree of data collapse is somewhat poor for 12 kW plasma, the similarity of the radial profiles exists in the near field of the plasma jet. It is also interesting to note that the radial spread of the profiles is small and such that the nozzle exit diameter is a sufficient length scale to collapse the data. It should be cautioned here also that these profiles represent partial profiles as the employed measurement technique cannot resolve the low-temperature regions. With these radial and axial distributions, the plasma temperature field can be empirically correlated as

$$T = \left[9.48\cdot10^6 \frac{(P_{el}\eta_{pl})^{1/4}}{V_{Ar}} \frac{1}{(z+9.13)^{1.35}} + 300\right] \exp\left(-4\frac{r^2}{d^2}\right) \quad \text{(Eq 6)}$$

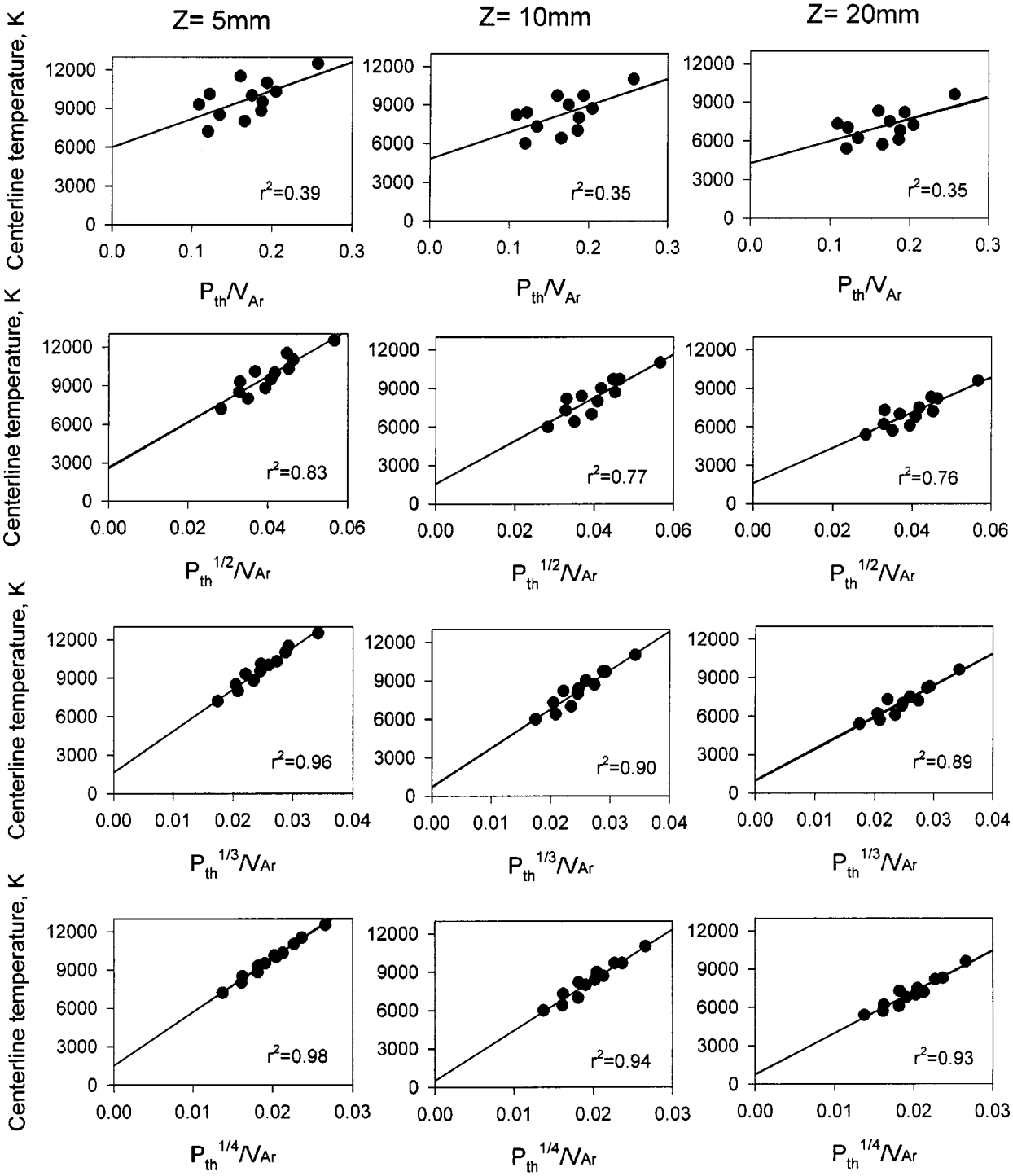

Fig. 9 Correlation of measured plasma centerline temperatures at different input powers, gas flow rates, and compositions

The ability of this correlation to reproduce the measured data is judged to be better than 20% for the 36 kW power input level. It should be noted that this correlation should only be used in the parameter region of the experiments in this study.

In order to explore the effects of plasma fluctuations, a set of experiments were performed, where one of the Ar-I emission lines (λ = 420.067 nm) was monitored by a fast photomultiplier detector. Figure 12 shows the photomultiplier output voltage that is proportional to the line emission intensity. In this figure, the background intensity level was subtracted from the raw signal in the same way as discussed earlier. In Fig. 12(a), the large amplitude intensity fluctua-

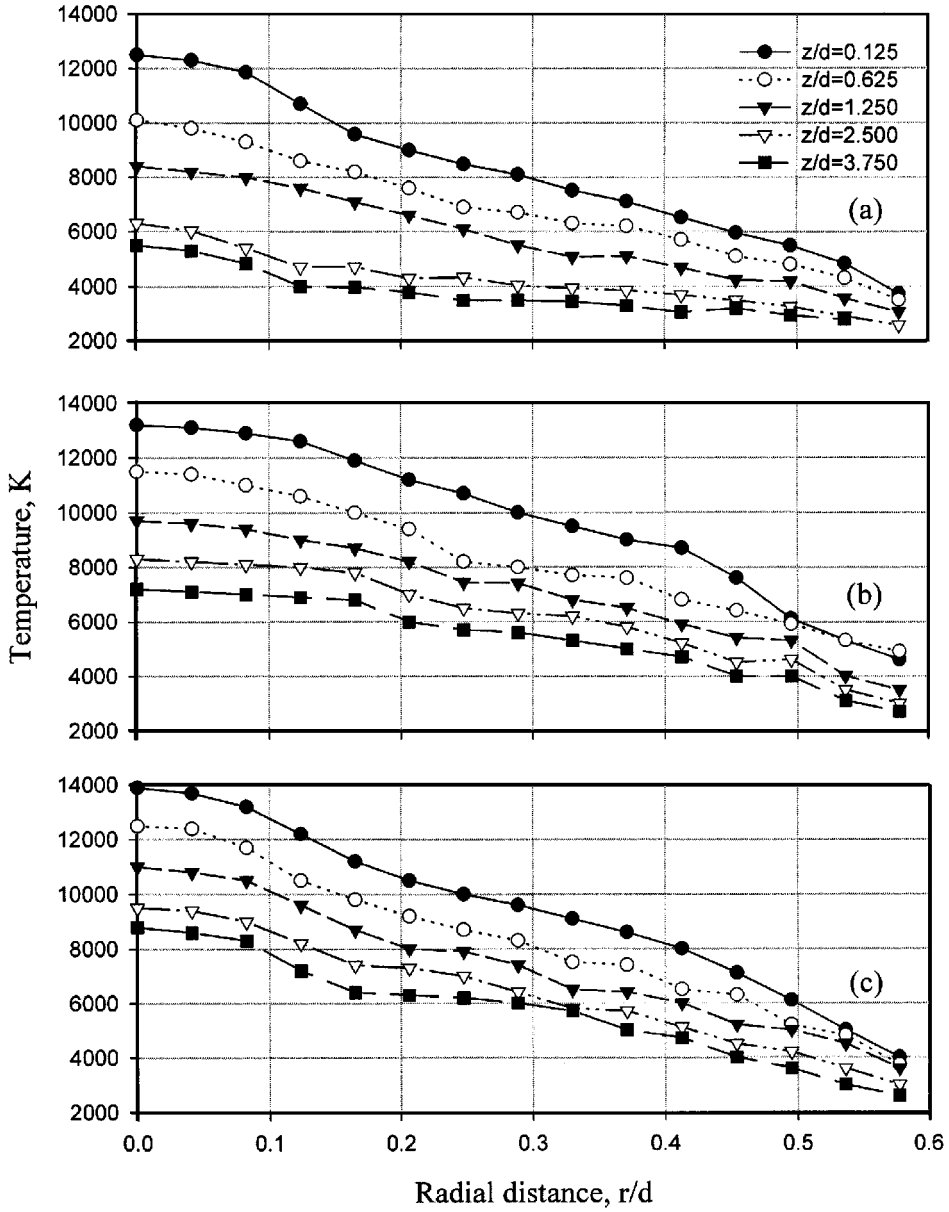

Fig. 10 Radial temperature distributions at different axial locations along the Ar/H_2 plasma jets with argon mole fraction of 0.8: (**a**) 12 kW, (**b**) 24 kW, and (**c**) 36 kW. The lines through the data represent the radial distribution in Eq 6

tions (up to 135% of the mean, peak to peak) are observed for the case of 20% volume fraction of H_2. These fluctuations with a frequency of 5.2 kHz are believed to be a result of the arc root instabilities and the associated "cold" and "hot" spots going through the measurement volume. As the steady-state measurements of temperature are biased toward the higher temperatures, the apparent increase of temperature in the time-averaged measurements is believed to be due to these high amplitude fluctuations. For the case of pure argon shown in Fig. 12(b), the fluctuation amplitude is much less, whereas the frequency has increased to about 34 kHz. In this case, the time-averaged temperature measurements are not affected as much by the fluctuations. These fluctuations could lead to overestimation of the time-averaged plasma temperatures in H_2 seeded plasmas based on emission spectroscopy.

4. Concluding Remarks

A comprehensive characterization of temperature field in argon/hydrogen DC arc plasma jets has been conducted using the emission spectroscopy of Ar-I species. The experiments involved imaging plasma radiation along a radial chord onto a spectrometer, which resolved it into its spectral features. Boltzmann distribution of the excited Ar-I species was the basis of temperature measurement. The variation of plasma axial and radial temperature distributions was measured as a

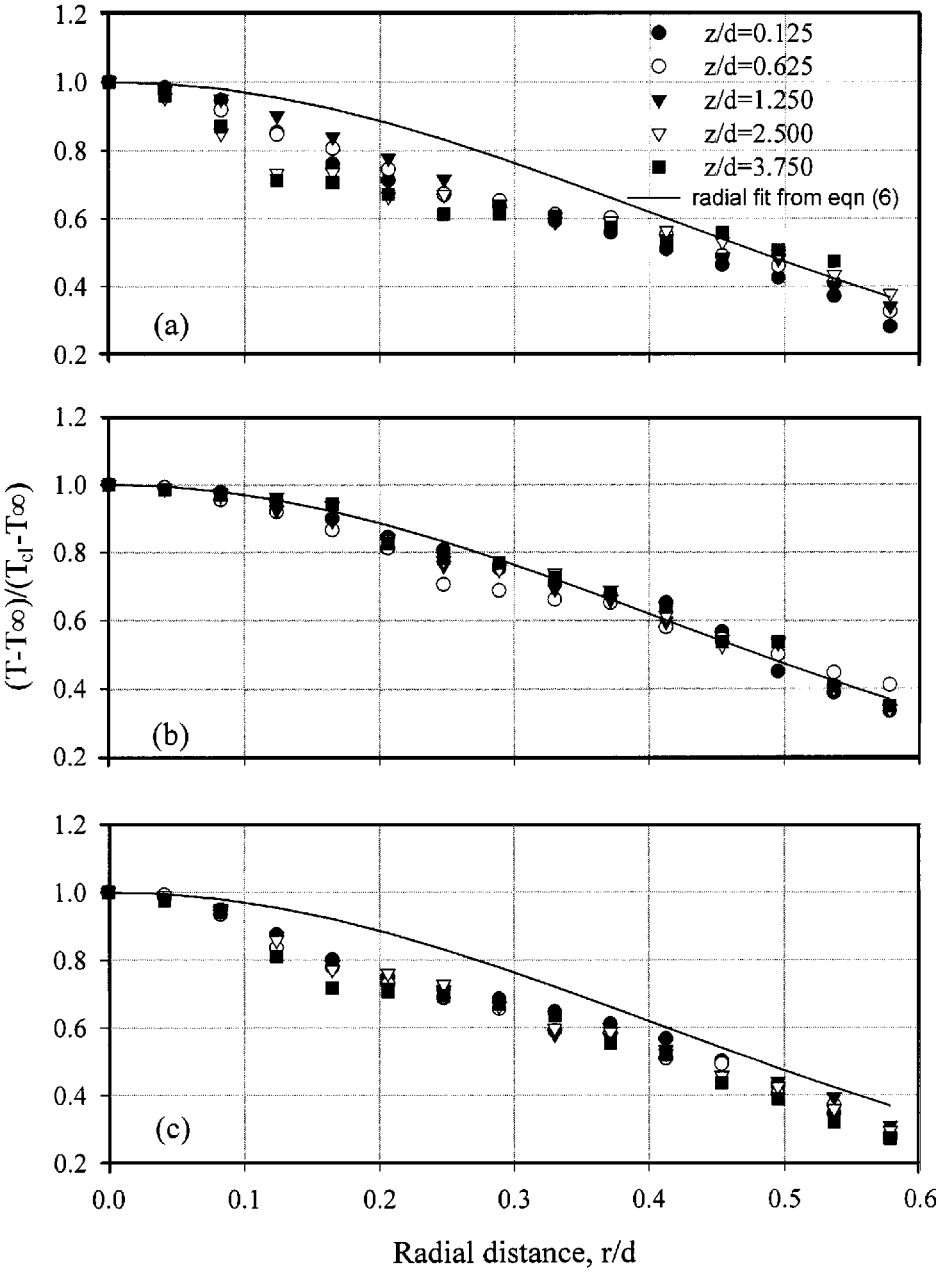

Fig. 11 Normalized distribution of radial temperature profiles at different axial locations. T_{cl} is the centerline temperature at that axial location, and T is the ambient temperature taken as 300 K: (**a**) 12 kW, (**b**) 24 kW, and (**c**) 36 kW

function of plasma input power, total gas flow rate, and the binary gas composition of argon and hydrogen. The time-averaged plasma gas temperatures increase with increasing plasma input power, increasing hydrogen content of the plasma gas, and decreasing total gas flow rate. Plasma temperatures decrease progressively with increasing distance from the nozzle exit. The peak temperatures near the nozzle exit are in the range of 12,500 to 14,000 K. The radial temperature profiles show an approximate self-similarity in the near field. Based on these temperature measurements, an empirical correlation of the temperature field is given. It is anticipated that these data and correlation will be useful for model comparisons as well as in choosing locations where different materials can be introduced into the plasma jets. This is particularly important for nanostructured materials that loose their structure when melted upon being exposed to high plasma temperatures. Finally, time-resolved measurements of Ar-I emission intensities showed that addition of hydrogen results in the amplification of fluctuations in the emission intensity at a frequency of about 5.2 kHz. This suggests that Ar/H_2 plasma temperatures will have a higher degree of fluctuation than will those of pure argon.

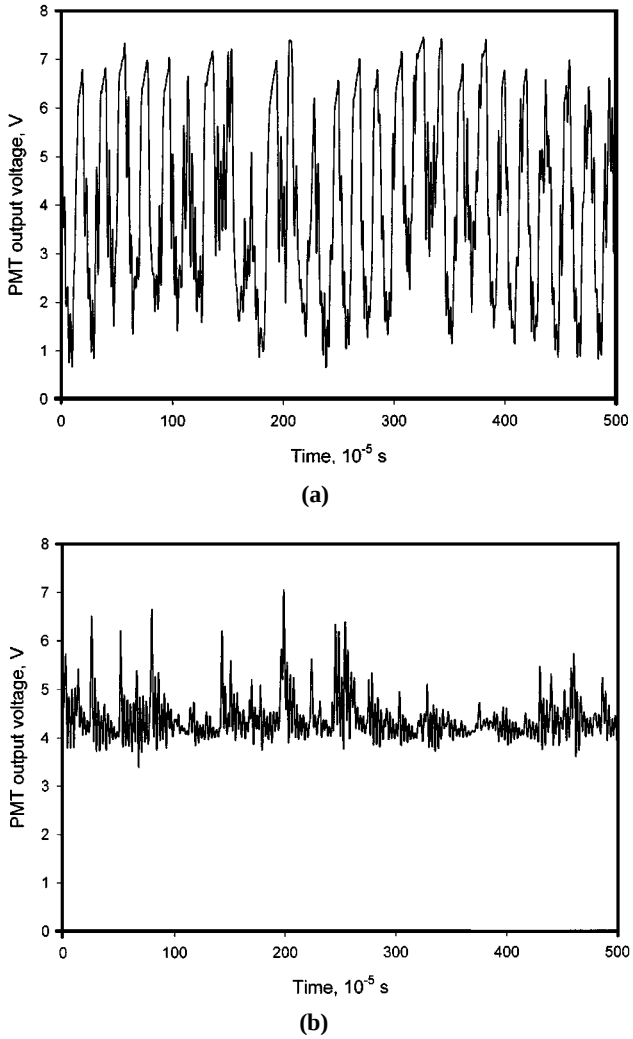

Fig. 12 Time-resolved Ar-I emission intensity at 36 kW power input: (**a**) $Y_{Ar} = 0.8$ and $Y_{H2} = 0.2$; and (**b**) $Y_{Ar} = 1.0$ and $Y_{H2} = 0.0$

Acknowledgments

Research reported herein was sponsored by the Office of Naval Research under Grant No. N00014-97-0843 under the direction of Dr. Lawrance Kabakoff. The authors acknowledge the useful and illuminating discussions with Professor Lutz Huewel, Wesleyan University, and Professor Marshall Long, Yale University.

References

1. L. Pawlowski: *The Science and Engineering Thermal Spray Coatings*, John Wiley and Sons, New York, NY, 1995.
2. A.H. Dilawari, J. Szekely, and R. Westhoff: *Plasma Chem. Plasma Proc.*, 1990, vol. 10 (4), pp. 501–13.
3. M.I. Boulos, P. Fauchais, and E. Pfender: *Thermal Plasmas*, Plenum Press, New York, NY, 1994, vol. 1.
4. P.W.J.M. Boumans: *Theory Spectrochemical Excitation*, Plenum Press, New York, NY, 1966.
5. N.K. Joshi, S.N. Sahasrabudhe, K.P. Sreekumar, and N. Venkatramani: *Measurement Sci. Technol.*, 1997, vol. 8, pp. 1146–50.
6. A.H. Dilawari, J. Szekely, J. Batdorf, R. Detering, and C.B. Shaw: *Plasma Chem. Plasma Proc.*, 1990, vol. 10 (2), pp. 321–37.
7. S.C. Snyder, L.D. Reynolds, G.D. Lassahn, J.R. Fincke, and C.B. Shaw: *Phys. Rev. E*, 1993, vol. 47 (3), pp. 1996–2005.
8. A.B. Murphy and P. Kovitya: *J. Appl. Phys.*, 1993, vol. 73 (10), pp. 4759–69.
9. A. Vardelle, J.M. Barronnet, M. Vardelle, and P. Fauchais: *IEEE Trans. Plasma Sci.*, 1980, vol. PS-8 (4), pp. 417–24.
10. W.L. Wiese, J.W. Brault, K. Danzmann, V. Helbig, and M. Kock: *Gen. Phys., Phys. Rev. A*, 1989, vol. 39 (5), pp. 2461–71.
11. C.J. Dash: *Appl. Optics*, 1992, vol. 31 (8), pp. 1146–52.
12. F.L. Mohler: *Temperature, Its Measurement and Control in Science and Industry Symp.*, Washington, D.C., Reinhold Publishing Company, New York, NY, 1939, p. 734.
13. W. Lochte-Hotgreven: *Temperature, Its Measurement and Control in Science and Industry Symp.*, Washington, D.C., Reinhold Publishing Company, New York, NY, 1954, p. 413
14. C.E. Moore: *Atomic Energy Levels*, NSRDS, Washington, DC, 1971, vol. 1, pp. 211–15.